

QAOA pseudo-Boltzmann states

Pablo Díez-Valle,^{1,*} Diego Porras,¹ and Juan José García-Ripoll¹

¹*Instituto de Física Fundamental IFF-CSIC, Calle Serrano 113b, Madrid 28006, Spain*

In this letter, we provide analytical and numerical evidence that the single-layer Quantum Approximate Optimization Algorithm (QAOA) on universal Ising spin models produces thermal-like states with Gaussian perturbations. We find that these pseudo-Boltzmann states can not be efficiently simulated on classical computers according to state-of-art techniques, and we relate this distribution to the optimization potential of QAOA. Moreover, we observe that the temperature depends on a hidden universal correlation between the energy of a state and the covariance of other energy levels and the Hamming distances of the state to those energies.

Introduction.— The Quantum Approximate Optimization Algorithm (QAOA) is a variational framework for the solution of combinatorial optimization problems in hybrid quantum computers [1]. The algorithm works by optimizing a trial wavefunction that alternates evolution with a simple mixing Hamiltonian and the problem Hamiltonian we wish to optimize. It has been shown that a single-layer ansatz already engineers a quantum probability distribution that is classically hard to sample [2]. This formal sampling advantage may or may not translate into a practical advantage in the optimization scenario, where there may be better classical [3] and quantum algorithms [4], and the variational ansatz may fail to reach the ground state due to high constraint density [5] or symmetries [6].

In this work, we connect the sampling advantage and the optimization properties, studying a simple, single-layer generalization of the QAOA ansatz. We study its performance both from the optimization point of view—i.e. the probability to find the ground state—and also by understanding the types of states it prepares—i.e. the IQP-like probability distributions that are hard to sample, according to Ref. [2].

Our study shows that single-layer QAOA-like optimization creates pure states where the probability of each Hamiltonian eigenstate approaches a Boltzmann distribution with Gaussian perturbations. Averaged over replicas, the temperature depends on the optimization angles, and the type and size of the problem. This result is confirmed for QUBO, Max-Cut and random Ising models in arbitrary dimensions. In these scenarios, we find that these *pseudo-Boltzmann* states exhibit a quadratic advantage over classical sampling strategies which include uniform sampling and classical Monte Carlo. The advantage is an algebraic enhancement of the ground-state probability distribution $\mathcal{O}(2^{N/2})$, similar to Grover-like search algorithms.

The structure of this work is as follows. First, we introduce the formulations of random QUBO, MaxCut, and random Ising models, and the graphs in which they will be embedded. We then introduce a convenient generalization of the QAOA single-layer circuit, showing numerical evidence that these are *pseudo-Boltzmann* states

with an average temperature that is constant over replicas and scales favorably with the problem size, enhancing the probability to find the ground state. We also provide a semi-analytical interpretation of the pseudo-Boltzmann states, as a result of quantum interference in energy space. We show that the single-layer variational ansatz acts as an interferometer which macroscopically shifts probability to the lower or higher energy states, depending on the choice of angles. The efficiency of this process depends on a hidden correlation between the eigenenergies of the problem and the Hamming distance between those eigenstates and other energy levels. Indeed, the degree of correlation lays behind the effective temperature of the pure state. We close this work with a discussion of the connections between the sampling advantages and actual advantages in optimization, with an outlook for further impact of these results.

Optimization problems.— We consider three families of binary combinatorial optimization problems, QUBO [7, 8], MaxCut [9–11] and random Ising models [12], all of which are NP-hard and have been used to benchmark variational algorithms. All these problems have an associated classical energy function, defined either in binary variables $\mathbf{x} \in \{0, 1\}^N$, or in terms of spins $\sigma^z = (2\mathbf{x} - 1)$.

$$E(\mathbf{x}) = \sum_{i,j=1}^N x_i Q_{ij} x_j = \sum_{i,j=1}^N \sigma_i^z J_{ij} \sigma_j^z + \sum_{i=1}^N h_i \sigma_i^z, \quad (1)$$

where $h_i = \sum_j Q_{ij}$, $J_{i \neq j} = Q_{ij}$ and $J_{ii} = 0$.

These problems are specified by an undirected graph with N vertices, connected by undirected edges $i \leftrightarrow j$ wherever the edge's weight is not zero $J_{ij} = J_{ji} \neq 0$ [cf. Fig. 1]. The goal is to assign each vertex a value 0 or 1 ($\sigma^z = -1$ or $+1$ in spin notation) as to minimize the Hamiltonian. Additionally, we consider problems on two families of random graphs, *Gnm random graphs*, also known as *Erdős-Rényi graphs* [cf. Fig. 1a], which fix the total number of edges M (or the density $\rho = 2M/(N^2 - N) \in [0, 1]$) and *random regular graphs* [cf. Fig. 1b], which instead fix the coordination number or degree Z of the N vertices.

These graphs are sampled using the Python package *networkx* [13], with 500 random instances for each config-

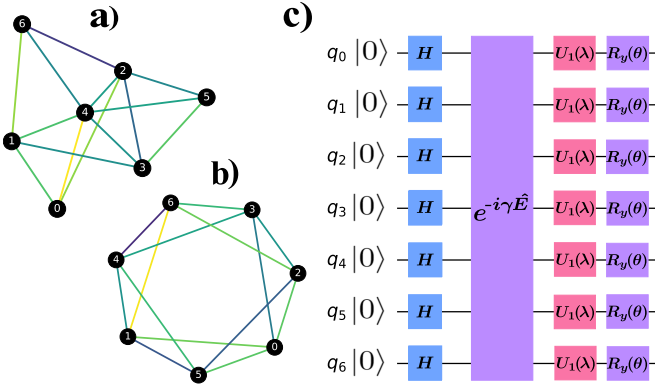


FIG. 1. (a) Example of a Gnm random graph of 7 nodes and density $\rho = 0.68$ (14 edges). (b) Example of a regular graph of 7 nodes and degree $Z = 4$ (14 edges). (c) The circuit of a single layer of the extended QAOA (see Eq. (2)) (Color online).

uration. Once the topology is fixed, we generate the coefficients of the Hamiltonian (1). In QUBO, the nonzero values of Q_{ij} are randomly drawn from a normal distribution $N(\mu = 0, \sigma)$ with zero average μ and variance σ . In MaxCut, we set $h = 0$ and sample J_{ij} with a normal distribution $N(0, \sigma)$. When the problem is fully connected, i.e. when we have all-to-all couplings, we recover the standard Sherrington-Kirkpatrick model [14]. Finally, the random Ising model samples both J and h with the same distribution $N(0, \sigma)$.

Single-layer QAOA.— Let us introduce a generalization of the QAOA ansatz, consisting of a layer of Hadamard gates $H^{\otimes N}$, followed by evolution with the Hamiltonian \hat{E} and single-qubit rotations $R_y^{\otimes N}$ and $U_1^{\otimes N}$, as shown in Fig. 1c. Therefore, the resultant state is given by:

$$|\Psi(\gamma, \theta, \lambda)\rangle \equiv R_y(\theta)^{\otimes N} U_1(\lambda)^{\otimes N} e^{-i\gamma\hat{E}} H^{\otimes N} |0\rangle^{\otimes N}, \quad (2)$$

with $R_y(\theta) \equiv \exp(-i\frac{\theta}{2}\sigma_y)$, $U_1(\lambda) \equiv \exp(-i\frac{\lambda}{2}\sigma_z)$, where $\sigma_{y,z}$ are the Pauli matrices. Here $\gamma, \theta > 0$ are variational parameters, while the phase λ controls the optimization direction. Note that, since measurements are not affected by local phases, the value $\lambda = \pm\frac{\pi}{2}$ is equivalent to a single layer QAOA [1].

Circuit (2) acts as an interferometer in energy space, amplifying the probability amplitude of the states with high or low energy for $\lambda = \pi/2$ or $-\pi/2$, respectively. This can be seen for a single two-level system $\hat{E} = \frac{1}{2}\Delta\sigma^z$, where the probability $P(s)$ to measure state $|s = \pm 1\rangle$ is

$$P_s = \frac{1}{2} (1 - s \sin(\theta) \cos(\gamma\Delta + \lambda)). \quad (3)$$

This probability is maximized for the ground ($s = -1$) and excited ($s = +1$) state for $\lambda = -\frac{\pi}{2}$ and $\lambda = +\frac{\pi}{2}$, respectively, using the optimal angles $\theta = \frac{\pi}{2}$ and $\gamma = \frac{\pi}{2\Delta}$.

Pseudo-Boltzmann states.— We have applied Eq. (2) to the variational minimization of QUBO, MaxCut and

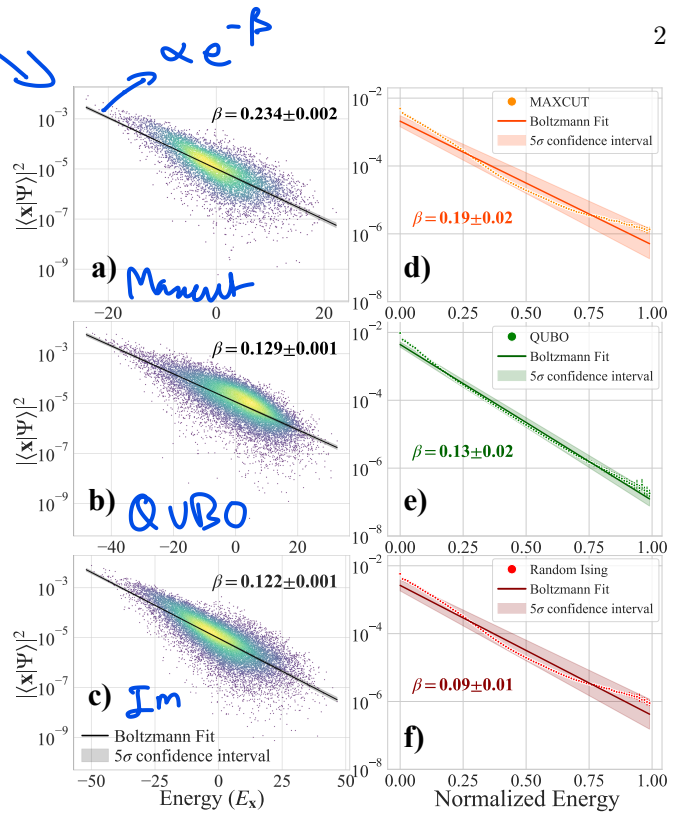


FIG. 2. Eigenstate probabilities (dots) and fitted Boltzmann distribution (line) for ansatz 2 with optimal angles in (a,d) Max-Cut, (b,e) QUBO and (c,f) Random Ising 14 qubits problems on Gnm random graphs with density equal to 0.9. In (d,e,f) we normalized the energies and computed the probabilities (dots) over 100 energy intervals, averaged over 500 replicas. We show these values, together with a fit to a Boltzmann distribution. All fits in (a-f) are plotted with a 99% confidence interval (Color online).

random Ising problems ($\lambda = -\pi/2$). We studied problems from 6 to 20 qubits, in Gnm random and regular graphs of varying density and coordination number, sampling also different parameters of the random Hamiltonian, with the distributions mentioned above. For each problem, we obtained numerically the angles $\{\theta, \gamma\}$ that maximized the ground state probability. We then computed the enhancement in the ground state probability with respect to uniform sampling, $\xi = |\langle x_0 | \Psi \rangle|^2 2^N$, and also reconstructed the probability distribution $P(E) = \sum_x \delta(E - E_x) |\langle x | \Psi \rangle|^2$ created by QAOA in energy space.

Figs. 2a-c show the optimized QAOA states for instances with 14 qubits of random (a) MaxCut, (b) QUBO and (c) random Ising problems. Even though they are pure states, the probability of the different eigenstates $|\langle x | \Psi \rangle|^2$ fluctuates around the straight line given by a Boltzmann distribution $|\langle x | \Psi \rangle|^2 \sim \exp(-\beta E_x)$ with inverse temperature β . This is what we call *pseudo-Boltzmann* states. As shown in this figure, this fit has a high confidence and correlation, and the actual probabilities resemble $P(E) \sim \exp(-\beta E) \rho(E)$, with a density of states $\rho(E)$ similar to a normal distribution, where the

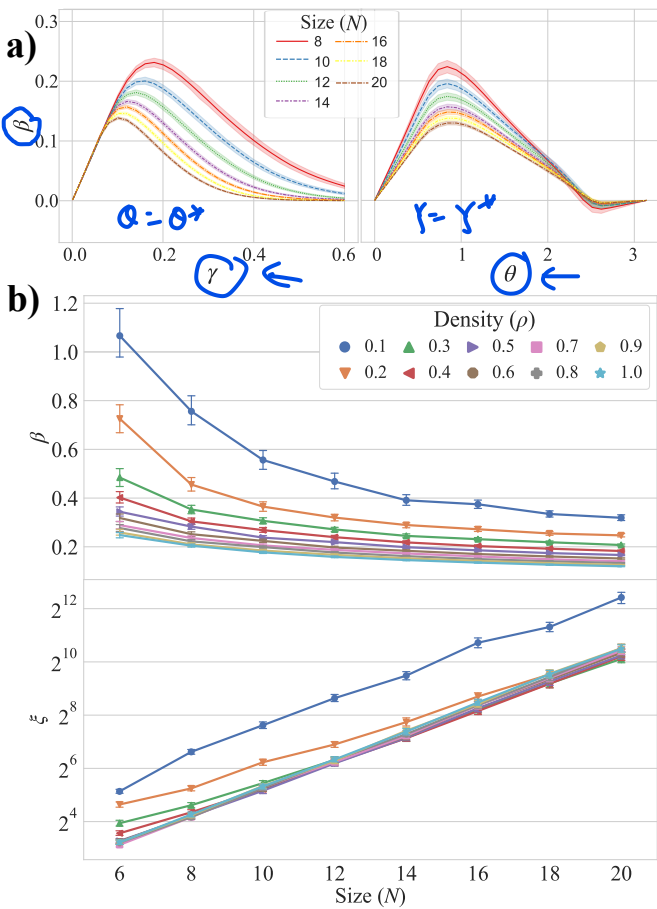


FIG. 3. (a) Effective temperature β after one-layer QAOA for QUBO problems on Gnm random graphs with density equal to 0.9 and different number of nodes, as a function of the QAOA angles. When varying γ , we set θ to its optimal value, and vice versa. The results show the average of 500 instances and a 99% confidence interval. (b) Effective temperature β and ground state amplitude enhancement after one-layer QAOA with optimal angles for QUBO problems on Gnm random graphs (Color online).

macroscopic region of intermediate energies (see below) dominates the tendency.

Inspired by this, we averaged the distribution over replicas $\langle P(E) \rangle$, sampling 500 instances for each problem size, normalizing the energies to the $[0, 1]$ interval, and averaging the probabilities over 100 sub-intervals. The result was fitted to a rescaled Boltzmann distribution, now independent of the Hamiltonian norm. Figs. 2d-f show three fits for the three families of random problems, for $N = 14$ spins. The average β is slightly lower than the one of individual instances, because of the energy normalization. We also notice that the QUBO model has the highest correlation.

The effective temperature of the pseudo-Boltzmann state is controlled by the variational angles and the problem size. As shown in Fig. 3a, β grows linearly with γ and θ until it reaches a maximum at which the Boltzmann

	Optimal γ	ξ	β
Gnm Random Graphs	$\frac{\chi_\gamma}{\sigma\sqrt{(N-1)\rho}}$	$\sqrt{2^N}$	$\frac{\chi_\beta}{\sigma\sqrt{(N-1)\rho}}$
Regular Graphs	$\frac{\chi_\gamma}{\sigma\sqrt{Z}}$	$\sqrt{2^N}$	$\frac{\chi_\beta}{\sigma\sqrt{Z}}$
General Graphs	$\frac{\chi_\gamma\sqrt{N}}{\sigma\sqrt{2M}}$	$\sqrt{2^N}$	$\frac{\chi_\beta\sqrt{N}}{\sigma\sqrt{2M}}$

TABLE I. Approximated trends of the single-layer QAOA that we observe when N is sufficiently large, as a function of the problem parameters [15]. These results were obtained for three families of combinatorial optimization problems: Max-Cut, QUBO, and random Ising models. The optimal θ converges to ≈ 0.93 when $h = 0$ (MaxCut), to $\approx \pi/3$ when the interaction matrix J and h are correlated (QUBO), and to ≈ 0.95 when they are not (random Ising), regardless of the graph class. ρ , Z , and M denotes the density, the degree, and the total number of edges of the graph respectively.

distribution breaks down. This is the point at which the interferometer wraps around in energy space, which happens for $\theta \simeq \pi/3$ and for a Hamiltonian angle that in the case of highly connected graphs decreases with problem size $\gamma \sim \mathcal{O}(N^{-1/2})$. In this case the inverse temperature also decreases with the number of spins $\beta \sim \mathcal{O}(N^{-1/2})$, but this gentle slow down still allows an exponential enhancement of the ground state population $\xi \sim \mathcal{O}(2^{N/2})$. Similar behaviors were obtained for all graphs and problems, with varying scalings depending on the graph parameters. Table I summarizes our fits for two families of graphs for the three classes of problems studied in this manuscript.

Derivation of pseudo-Boltzmann states.— The QAOA circuit (2) works by creating a uniform superposition of all problem eigenstates \mathbf{x} , which evolve for a time γ with their energies $E_{\mathbf{x}}$ and later interfere in the local rotations λ and θ . We can understand the amplitude of final states $F(\mathbf{x}) = \langle \mathbf{x} | \Psi \rangle$ as the average [15]

$$F(\mathbf{x}) \propto \langle \exp(H_{\mathbf{xx}'}(-i\lambda - r_\theta) - i\gamma E_{\mathbf{x}'}) \rangle_{\mathbf{x}'} . \quad (4)$$

Here $r_\theta = -\log(\tan(\theta/2))$, $H_{\mathbf{xx}'}$ is the Hamming distance between two bit strings, and we average uniformly over all spin configurations \mathbf{x}' .

In the limit of large problems, we can replace the average over configurations by an average over a continuous probability distribution $p(H, E, \mathbf{x})$ that samples different energies E and the Hamming distances H from the state \mathbf{x} to those energies. Numerically we find that the distribution $p(H, E, \mathbf{x})$ is approximately a sum of a small number of Gaussians, where the number depends on the symmetries and degeneracy of the problem. For the models presented on this manuscript one or two Gaussian are sufficient [15]. Every Gaussian is defined by

$$p(H, E, \mathbf{x}) \propto e^{-\frac{1}{2(1-\rho^2)} \left[\left(\frac{E}{\sigma_E} \right)^2 + \left(\frac{H - \mu_H}{\sigma_H} \right)^2 - 2\rho \frac{E(H - \mu_H)}{\sigma_E \sigma_H} \right]} , \quad (5)$$

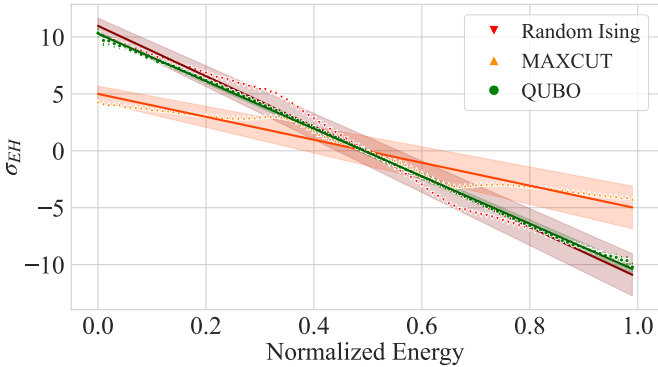


FIG. 4. Average covariance σ_{EH} as a function of the normalized energy of the state E_x over 300 replicas for QUBO, MaxCut and random Ising problems on Gnm random graphs with 14 nodes. Note that $\sigma_{EH} \equiv \sigma_{EH+}$ for degenerate problems, as explained in [15]. The fits show the 99% confidence interval around the linear fits (Color online).

where the energy and the Hamming distances are centered on $\mu_E = 0$ and μ_H respectively, σ_E and σ_H are the standard deviations, and we have a correlation factor for each of the Gaussians

$$\rho(\mathbf{x}) = \frac{1}{\sigma_E \sigma_H} \sigma_{EH}(\mathbf{x}), \quad (6)$$

where $\sigma_{EH}(\mathbf{x})$ is the covariance. Empirically, this correlation factor is small, but still dominates the integral in $F(\mathbf{x})$, so that we can write [15]

$$|F(\mathbf{x})|^2 \propto e^{-2\gamma\lambda\sigma_{EH}(\mathbf{x})}, \quad (7)$$

up to a normalization factor. Finally, as shown in Fig. 4 there is a clear correlation between σ_{EH} , calculated by numerical fit to (5), and the energy of the state E_x , with small random fluctuations ω around $\sigma_{EH} \sim -cE_x$. This allows us to write

$$|F(\mathbf{x})|^2 \propto e^{-\beta E_x + \beta \omega/c}, \quad (8)$$

with the effective temperature $\beta = -2c\gamma\lambda$. Note how different problems (QUBO, MaxCut, random Ising) have different degrees of correlation, but seem to collapse into universal curves. Moreover, we interpret that the degeneracy of the energy levels explains a worse fits to a Boltzmann distribution for MaxCut and random Ising due to the existence of small corrections [15] [cf. Fig. 2].

Summary and discussion.— It has been shown that single-layers QAOA circuits have a quantum advantage, in the sense that they are classically hard to sample [2], for if they were not, the polynomial hierarchy would collapse. This result is related to the conjecture that the complex partition function of an Ising model, which is recreated by the circuits, is hard to sample [16].

These ideas have motivated our investigation of the structure of the states created by a QAOA single-layer

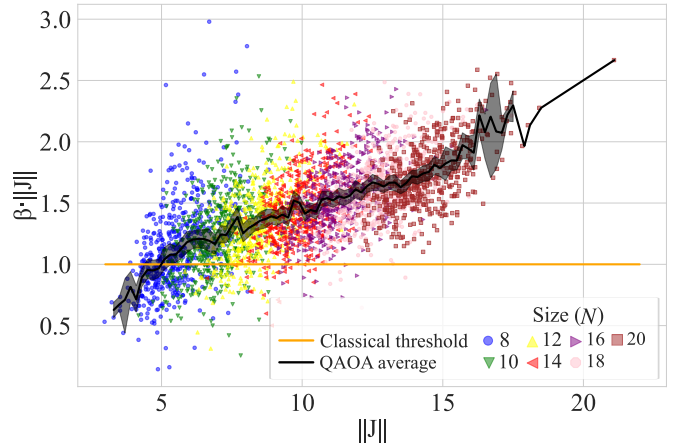


FIG. 5. Effective temperatures β after single-layer QAOA with optimal angles, as a function of the interaction matrix J norm for QUBO problems with density equal to 1. The dots display the results for 500 instances for each problem size, which grows with the J norm. We show the average of these results (black line) and the threshold given by Monte Carlo methods (orange line) which demonstrates that the distributions obtained with one-layer QAOA are hard to sample classically (Color online).

circuit, looking for a quantitative gap between the classical and quantum simulations. We have performed this study for NP-hard problem Hamiltonians on random graphs of different type and dimensions. Our simulations and the accompanying theory reveal that single-layer QAOA circuits sample the eigenstates of a problem Hamiltonian according to a Boltzmann distribution with fluctuations. When averaged over replicas, the effective temperature of this *pseudo-Boltzmann* pure state scales favorably with the problem size, enhancing the probability of finding the ground state by an algebraic factor $\xi \sim \mathcal{O}(2^{N/2})$, similar to Grover-type search algorithms.

It may be argued that uniform sampling is not the best strategy for combinatorial optimization problems and that one should compare with Markov Chain Monte Carlo algorithms (MCMC). Here we can show that the effective temperature β [cf. Table I] provided by QAOA can fall outside the rapid mixing regime $\beta \gtrsim 1/\|J\|$, in which state-of-the-art MCMC could approximate the pseudo-Boltzmann state [17]. As illustration of this fact, Fig. 5 shows the QAOA temperature for 3500 instances of different size of QUBO with density equal to 1, where $\beta \sim \mathcal{O}(N^{-1/2})$ as compared to $\|J\|^{-1} \sim \mathcal{O}(N^{-1})$. Already for 8 qubits the quantum state surpasses the classical threshold and grows with the above mentioned quadratic advantage.

The results in this work are built upon a qualitative understanding of the structure of eigenstates and their correlations in Ising-like spin models. This analysis merits further investigation, to understand whether the correlations that support QAOA's advantage may be trans-

latable to other scenarios and problems.

As outlook, this work may help develop a better understanding of multi-layer QAOA and adiabatic quantum computation. To be precise, our study has revealed that a single-step QAOA with very small angles approximates well a thermal distribution. Given that single-layer QAOA approximates a short-time step in adiabatic quantum evolution [1], it is natural to expect that one may relate a full adiabatic quantum protocol to a process that creates pseudo-Boltzmann states—with temperatures that now also will depend on the speed of the passage.

We believe that the generation of single-layer pseudo-thermal states is related to the success in approximating thermal states using QAOA-like variational ansätze with entropy and multiple layers of Hamiltonian evolution [18]. Indeed, a generalization of this work to many applications of the Hamiltonian may not only provide a rigorous explanation for [18] but also give insight on the nature of states created through imperfect adiabatic evolution.

We acknowledge Centro de Supercomputación de Galicia (CESGA) who provided access to the supercomputer FinisTerrae for performing simulations. We thank Fernando J. Gómez-Ruiz for critical reading of the manuscript. This work has been supported by European Commission FET Open project AVaQus Grant Agreement 899561, PGC2018-094792-BI00 (MCIU/AEI/FEDER,UE), Comunidad de Madrid Sinergicos 2020 project NanoQuCo-CM (Y2020/TCS-6545) and CSIC Quantum Technologies Platform PTI-001.

- [9] G. Nannicini, *Physical Review E* **99**, [10.1103/physreve.99.013304](https://doi.org/10.1103/physreve.99.013304) (2019).
- [10] K. J. Sung, J. Yao, M. P. Harrigan, N. C. Rubin, Z. Jiang, L. Lin, R. Babbush, and J. R. McClean, *Quantum Science and Technology* **5**, 044008 (2020).
- [11] M. P. Harrigan, K. J. Sung, and N. et.al, *Nature Physics* **17**, 332–336 (2021).
- [12] F. Barahona, *Journal of Physics A: Mathematical and General* **15**, 3241 (1982).
- [13] A. A. Hagberg, D. A. Schult, and P. J. Swart, in *Proceedings of the 7th Python in Science Conference*, edited by G. Varoquaux, T. Vaught, and J. Millman (Pasadena, CA USA, 2008) pp. 11 – 15.
- [14] D. Sherrington and S. Kirkpatrick, *Physical Review Letters* **35**, 1792 (1975).
- [15] See supplementary material for “qaoa pseudo-boltzman states” (2022).
- [16] M. J. Bremner, A. Montanaro, and D. J. Shepherd, *Physical Review Letters* **117**, [10.1103/physrevlett.117.080501](https://doi.org/10.1103/physrevlett.117.080501) (2016).
- [17] R. Eldan, F. Koehler, and O. Zeitouni, A spectral condition for spectral gap: Fast mixing in high-temperature ising models (2021), [arXiv:2007.08200 \[math.PR\]](https://arxiv.org/abs/2007.08200).
- [18] G. Verdon, M. Broughton, and J. Biamonte, A quantum algorithm to train neural networks using low-depth circuits (2019), [arXiv:1712.05304 \[quant-ph\]](https://arxiv.org/abs/1712.05304).

* pablo.diez@csic.es

- [1] E. Farhi, J. Goldstone, and S. Gutmann, A quantum approximate optimization algorithm (2014), [arXiv:1411.4028 \[quant-ph\]](https://arxiv.org/abs/1411.4028).
- [2] E. Farhi and A. W. Harrow, Quantum supremacy through the quantum approximate optimization algorithm (2019), [arXiv:1602.07674 \[quant-ph\]](https://arxiv.org/abs/1602.07674).
- [3] M. B. Hastings, Classical and quantum bounded depth approximation algorithms (2019), [arXiv:1905.07047 \[quant-ph\]](https://arxiv.org/abs/1905.07047).
- [4] D. Amaro, C. Modica, M. Rosenkranz, M. Fiorentini, M. Benedetti, and M. Lubasch, *Quantum Science and Technology* **7**, 015021 (2022).
- [5] V. Akshay, H. Philathong, M. Morales, and J. Biamonte, *Physical Review Letters* **124**, [10.1103/physrevlett.124.090504](https://doi.org/10.1103/physrevlett.124.090504) (2020).
- [6] S. Bravyi, A. Kliesch, R. Koenig, and E. Tang, *Physical Review Letters* **125**, [10.1103/physrevlett.125.260505](https://doi.org/10.1103/physrevlett.125.260505) (2020).
- [7] G. Kochenberger, F. Glover, and B. Alidaee et al., *OR Spectrum* **26**, 237 (2004).
- [8] G. Kochenberger, J. Hao, and F. Glover et al., *J Comb Optim* **28**, 58–81 (2014).

Supplementary material to “QAOA pseudo-Boltzmann states”

P. Díez-Valle¹, D. Porras¹, J. J. García Ripoll¹

¹*Instituto de Física Fundamental IFF-CSIC, Calle Serrano 113b, Madrid 28006, Spain*

3Qubit

I. Analytical probability amplitude

We now shall focus on how the amplitudes of the wavefunction transform

$$F(\mathbf{x}) \equiv \langle \mathbf{x} | \tilde{\Psi} \rangle = \left[\frac{1}{2^{N/2}} \sum_{\mathbf{x}'} \cos\left(\frac{\theta}{2}\right)^{N-H_{\mathbf{x},\mathbf{x}'}} \left(e^{-i\lambda} \sin\left(\frac{\theta}{2}\right) \right)^{H_{\mathbf{x},\mathbf{x}'}} e^{-i\gamma E_{\mathbf{x}'}} \right] \quad (9)$$

where $H_{\mathbf{x},\mathbf{x}'}$ is the Hamming distance between two configurations of bits \mathbf{x} and \mathbf{x}' , and $E_{\mathbf{x}'} = \langle \mathbf{x}' | H | \mathbf{x}' \rangle$ with H the Hamiltonian of the problem. As we can define

$$\cos\left(\frac{\theta}{2}\right) = R^{\frac{1}{2}} \exp\left(\frac{r}{2}\right), \quad \sin\left(\frac{\theta}{2}\right) = R^{\frac{1}{2}} \exp\left(-\frac{r}{2}\right), \quad (10)$$

then the amplitudes become

$$F(\mathbf{x}) = \left(\frac{R \exp(r)}{2} \right)^{\frac{N}{2}} \sum_{\mathbf{x}'} \exp [H_{\mathbf{x}\mathbf{x}'} (-i\lambda - r) - i\gamma E_{\mathbf{x}'}]. \quad (11)$$

Taking into account that there are 2^N possible \mathbf{x}' configurations:

$$F(\mathbf{x}) = (2R \exp(r))^{\frac{N}{2}} \langle \exp [H_{\mathbf{x}\mathbf{x}'} (-i\lambda - r) - i\gamma E_{\mathbf{x}'}] \rangle_{\mathbf{x}'}, \quad (12)$$

where $\langle \cdot \rangle_{\mathbf{x}'}$ is the average of the sum respect to \mathbf{x}' . If there is a probability distribution $p(H_{\mathbf{x},\mathbf{x}'}, E_{\mathbf{x}'}; \mathbf{x})$, which we can write in continuous form, then we may write:

$$F(\mathbf{x}) \propto (\exp(r))^{\frac{N}{2}} \int \int_{-\infty}^{\infty} \exp [H(-i\lambda - r) - i\gamma E] p(H, E; \mathbf{x}) dH dE, \quad (13)$$

where, from now on, $H \equiv H_{\mathbf{x}\mathbf{x}'}$, and $E \equiv E_{\mathbf{x}'}$. The form of p may differ depending on the degeneracy of the system.

Non-degenerate scenario

We have shown numerically that, when the energy levels are non-degenerate, the probability distribution $p(H, E; \mathbf{x})$ can be well approximated by a bivariate Gaussian where the covariance σ_{EH} depends on \mathbf{x} (see Fig. 6):

$$p(H, E; \mathbf{x})_{\rho} \approx \frac{1}{2\pi\sigma_E\sigma_H\sqrt{1-\rho^2}} \exp \left[-\frac{1}{2(1-\rho^2)} \left(\left(\frac{E}{\sigma_E} \right)^2 + \left(\frac{H-\mu_H}{\sigma_H} \right)^2 - 2\rho \frac{E(H-\mu_H)}{\sigma_E\sigma_H} \right) \right], \quad (14)$$

where

$$\mu_E = 0; \quad \mu_H = \frac{N}{2}; \quad \sigma_H = \frac{\sqrt{N}}{2}; \quad \rho = \frac{\sigma_{EH}(\mathbf{x})}{\sigma_E\sigma_H}. \quad (15)$$

Note that the correlation parameter ρ encapsulates the dependence in \mathbf{x} since the features of the spin model fix the rest of the values. Then, Eq. (13) and Eq. (14) lead to

$$|F(\mathbf{x})|^2 \propto \exp[Y], \quad (16)$$

with

$$Y = -\gamma^2 \sigma_E^2 + (r^2 - \lambda^2) \sigma_H^2 - 2r\mu_H - 2\gamma\lambda\rho\sigma_E\sigma_H. \quad (17)$$

From this equation, we can obtain several conclusions, such as the probability amplitude distribution as a function of energy (see appendix II).

Degenerate scenario

When the energy levels are degenerate, Hilbert space can be divided into two or more subspaces. For example, for the random MaxCut problems that we work with, the \mathbb{Z}_2 symmetry ensures that in some circumstances we have two of such spaces \mathcal{H}_+ , \mathcal{H}_- , so that the probability distribution $p(H, E; \mathbf{x})$ can be defined as the sum of the probability distribution of both subspaces:

$$p(H, E; \mathbf{x}) = p_+(H_{\mathbf{x}, \mathbf{x}'_+}, E_{\mathbf{x}'_+}; \mathbf{x}) + p_-(H_{\mathbf{x}, \mathbf{x}'_-}, E_{\mathbf{x}'_-}; \mathbf{x}) \quad (18)$$

where $\mathbf{x}'_m \in \mathcal{H}_m$ with $m \in \{+, -\}$. With an adequate (and always possible) selection of subspaces \mathcal{H}_+ , \mathcal{H}_- , we have found that these distributions can be well fitted by two shifted bivariate Gaussian distributions (see Fig. 6):

$$p_+(H, E; \mathbf{x})_{\rho_+} \approx \frac{1}{2\pi\sigma_E\sigma_H\sqrt{1-\rho_+^2}} \exp \left[-\frac{1}{2(1-\rho_+^2)} \left(\left(\frac{E}{\sigma_E} \right)^2 + \left(\frac{H - \mu_H + h_0}{\sigma_H} \right)^2 - 2\rho_+ \frac{E(H - \mu_H + h_0)}{\sigma_E\sigma_H} \right) \right], \quad (19)$$

$$p_-(H, E; \mathbf{x}) \approx p_+(-H + 2\mu_H, E; \mathbf{x})_{\rho_-}, \quad (20)$$

where $\mu_H = N/2$, $\rho_{\pm} = \frac{\sigma_{EH}^{\pm}(\mathbf{x})}{\sigma_E\sigma_H}$, and $h_0 > 0$ is a constant shift. Again, note that ρ_{\pm} encapsulates all dependence in \mathbf{x} . Therefore, from Eq. (13) and Eq. (18) we find that

$$|F(\mathbf{x})|^2 \propto \exp[Y'] \cdot (\cos[2h_0\lambda + r\gamma(\rho_+ + \rho_-)\sigma_E\sigma_H] + \cosh[2h_0r - \gamma\lambda(\rho_+ + \rho_-)\sigma_E\sigma_H]), \quad (21)$$

where $Y' \equiv -\gamma^2\sigma_E^2 + (r^2 - \lambda^2)\sigma_H^2 - 2r\mu_H + \gamma\lambda(\rho_- - \rho_+)\sigma_E\sigma_H$. The cosine is only an oscillatory term, so we note that the probability amplitude is described by a mixture of two Boltzmann-like exponentials at opposite temperature where instead of the energy we have the correlation factor ρ_{\pm} . Nevertheless, since $|\rho_{\pm}| \ll 1$ for most states, the h_0 -shift makes one of the exponentials dominant in the range of values given by our systems. Thus, in this regime

$$\begin{aligned} 2\cosh[2h_0r - \gamma\lambda(\rho_+ + \rho_-)\sigma_E\sigma_H] &= \exp[\beta'(\rho_+ + \rho_-) + 2h_0r] + \exp[-\beta'(\rho_+ + \rho_-) - 2h_0r] \\ &\approx \exp[\beta'(\rho_+ + \rho_-) + 2h_0r], \end{aligned} \quad (22)$$

with $\beta' \equiv -\gamma\lambda\sigma_E\sigma_H$. Then, from Eq. (21) and Eq. (22)

$$|F(\mathbf{x})|^2 \propto \exp[Y'] \cdot \exp[\beta'(\rho_+ + \rho_-)] = \exp[Y] \quad (23)$$

with

$$Y = -\gamma^2\sigma_E^2 + (r^2 - \lambda^2)\sigma_H^2 - 2r\mu_H - 2\gamma\lambda\rho\sigma_E\sigma_H, \quad (24)$$

where $\rho \equiv \rho_+$. Notice that we obtain the same probability amplitude as for the non-degenerate scenario (16), except for small corrections due to the mixture (22).

II. Boltzmann states from QAOA

To study the probability amplitude distribution of the energy states, we are just interested in terms of Eqs. (16, 23) with \mathbf{x} dependence. Therefore, on Eqs. (17, 24) the only significant part is

$$Y \approx -2\gamma\lambda\rho\sigma_E\sigma_H = -2\gamma\lambda\sigma_{EH},$$

and hence

$$|F(\mathbf{x})|^2 \propto \exp(-2\gamma\lambda\sigma_{EH}) \quad (25)$$

where $\sigma_{EH} = \sigma_{EH}(\mathbf{x})$. Let us recall that σ_{EH} is the covariance between the energy of a classical state \mathbf{x}' and the Hamming distance between \mathbf{x}' and the configuration of bits \mathbf{x} .

We have numerically observed a clear correlation between σ_{EH} and the energy of the state \mathbf{x} (see Figs. 4 and 6) so that we can write:

$$\sigma_{EH}(\mathbf{x}) = -c \cdot E_{\mathbf{x}} \pm \omega, \quad (26)$$

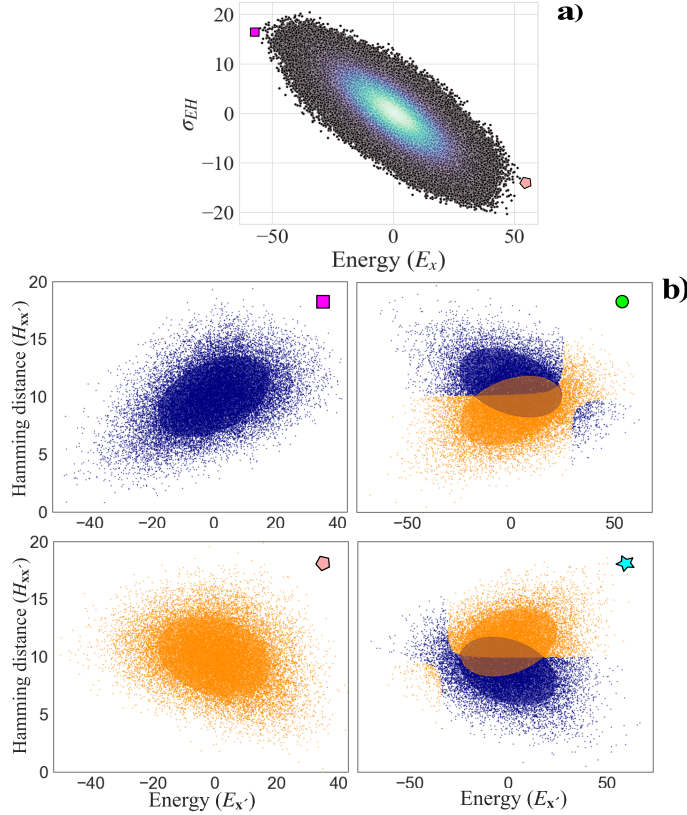


FIG. 6. (a) Correlation between the covariance σ_{EH} and energy E_x for one QUBO instance on Gnm random graph with 20 nodes. (b) Continuous probability distribution $p(H, E; \mathbf{x})$ estimated by 25000 samples drawn from a kernel density estimation (KDE). We show the distributions for one instance of (square and pentagon) non-degenerate QUBO and (circle and star) degenerate MaxCut model, where \mathbf{x} is (square and circle) the ground state, and (pentagon and star) the highest energy state of the system. Over these probability distributions, we plot the confidence ellipsoids of the fit to a Gaussian mixture obtained with Variational Inference (Color online).

where $c = cte > 0$, and ω is a stochastic value distributed with mean 0. Despite the presence of this ω randomness, the tendency (26) is manifest, and this correlation holds for all the studied families of Ising models.

Therefore, from Eq. (25) we get to express (2) as a thermal-like state:

$$|F(\mathbf{x})|^2 \propto \exp(-\beta E_{\mathbf{x}}) \pm \omega', \quad (27)$$

where $\omega' = \exp(\beta\omega/c)$, and $\beta = -2c\gamma\lambda$ with $c = cte > 0$. Note that ω' makes the probability amplitude a variable with some stochastic nature. However, the overall Boltzmann distribution is clear when the QAOA angles are in an optimal range [cf. Fig. 2]. Let us summarize how this Boltzmann distribution (27) is transformed when we modify the angles λ , and γ .

- λ : when $-\lambda = \frac{\pi}{2}$ we obtain a thermal state with temperature $T = \beta^{-1} = \frac{1}{c\pi\gamma}$ so that the maximum amplitude corresponds to the ground state of the system. When $\lambda = \frac{\pi}{2}$ we have an equivalent distribution but with a negative effective temperature so that the highest energy state has the largest amplitude.
- γ : for any $\gamma \in (0, t]$ ($t \in \mathbb{R}$, $\lambda > 0$) we get a *pseudo-Boltzmann state*, reaching the minimal temperature T when $\gamma = t$ for some value t . Over that limit t , in the non-degenerate scenario every term in Eq. (16) becomes negligible compared to $-\gamma^2\sigma_E^2$ and $|F(\mathbf{x})|^2 \approx cte$, and in the degenerate cases the approximation (22) also becomes inaccurate.

III. Approximated trends

We show in Figs. 7-12 the numerical evidence for the trends presented in table I. We include the results for all families of problems and random graph types analyzed in the paper.

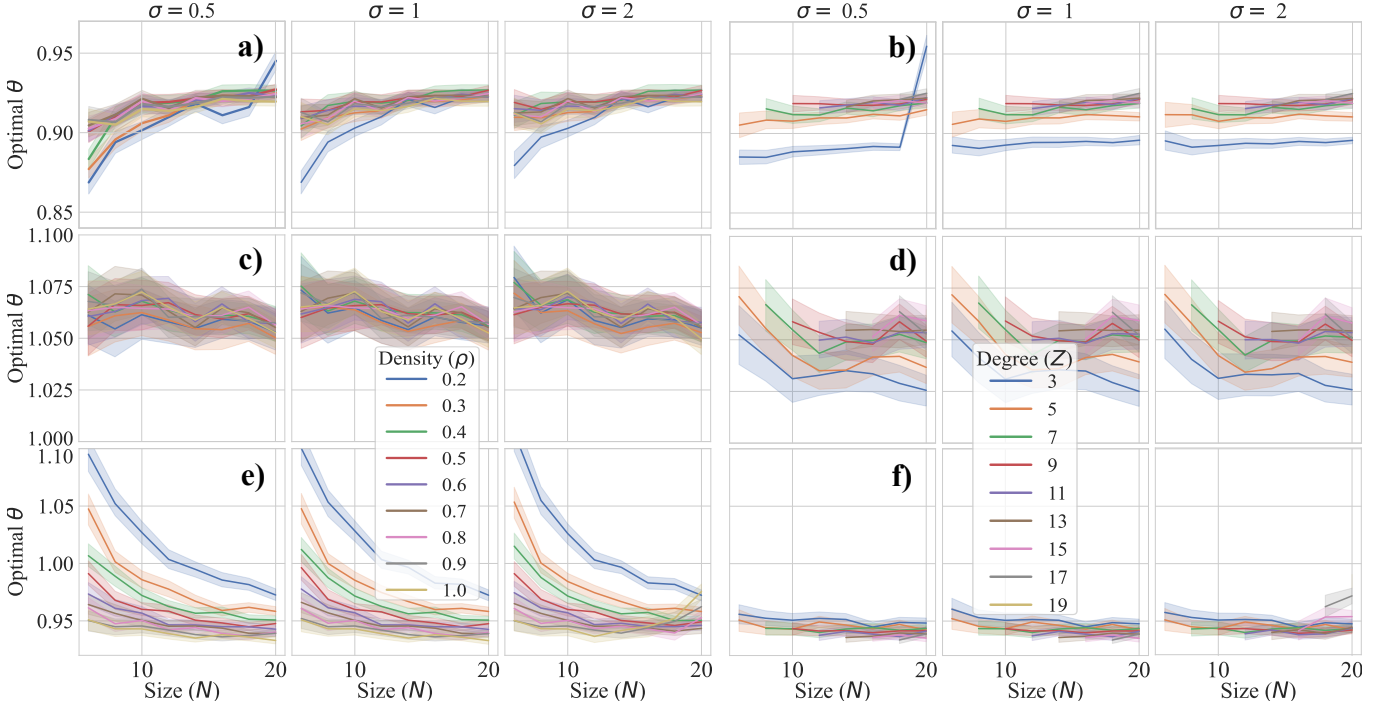


FIG. 7. Evidence that the optimal angle θ_{opt} of the single-layer QAOA converges to approximately a constant value. The results show the average of 500 instances and a 95% confidence interval for (a,b) MaxCut ($\theta_{opt} \approx 0.93$), (c,d) QUBO ($\theta_{opt} \approx \frac{\pi}{3}$), and (e,f) Random Ising model ($\theta_{opt} \approx 0.95$) problems on (a,c,e) Gnm random graphs and (b,d,f) regular graphs (Color online).

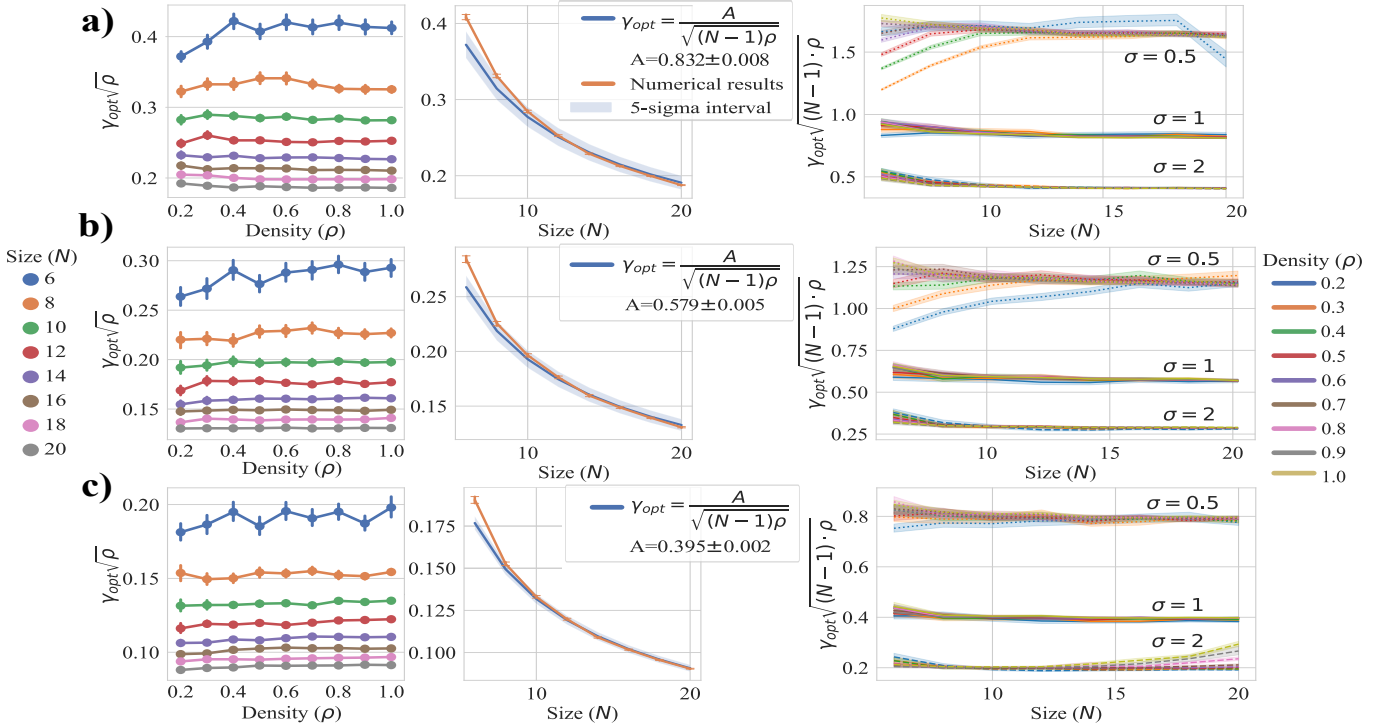


FIG. 8. Evidence that the optimal angle γ_{opt} of the single-layer QAOA scales as $\approx \frac{\chi_\gamma}{\sigma\sqrt{(N-1)\cdot\rho}} = \frac{\chi_\gamma\sqrt{N}}{\sigma\sqrt{2M}}$. The results show the average of 500 instances for (a) MaxCut ($\chi_\gamma = 0.832 \pm 0.008$), (b) QUBO ($\chi_\gamma = 0.579 \pm 0.005$), and (c) Random Ising model ($\chi_\gamma = 0.395 \pm 0.002$) problems on Gnm random graphs. The plots of the first and second columns were obtained with $\sigma = 1$ (Color online).

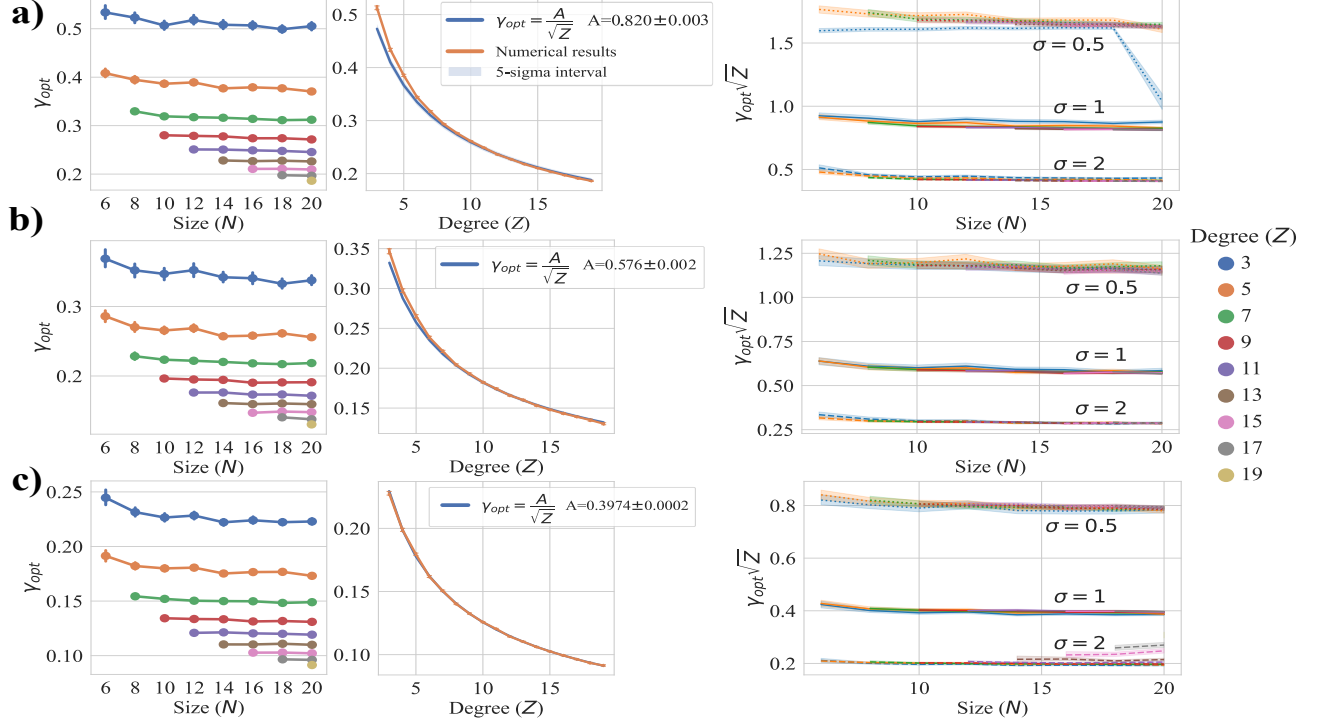


FIG. 9. Evidence that the optimal angle γ_{opt} of the single-layer QAOA scales as $\approx \frac{\chi_\gamma}{\sigma\sqrt{Z}} = \frac{\chi_\gamma\sqrt{N}}{\sigma\sqrt{2M}}$. The results show the average of 500 instances for (a) MaxCut ($\chi_\gamma = 0.820 \pm 0.003$), (b) QUBO ($\chi_\gamma = 0.576 \pm 0.002$), and (c) Random Ising model ($\chi_\gamma = 0.3974 \pm 0.0002$) problems on regular graphs (Color online).

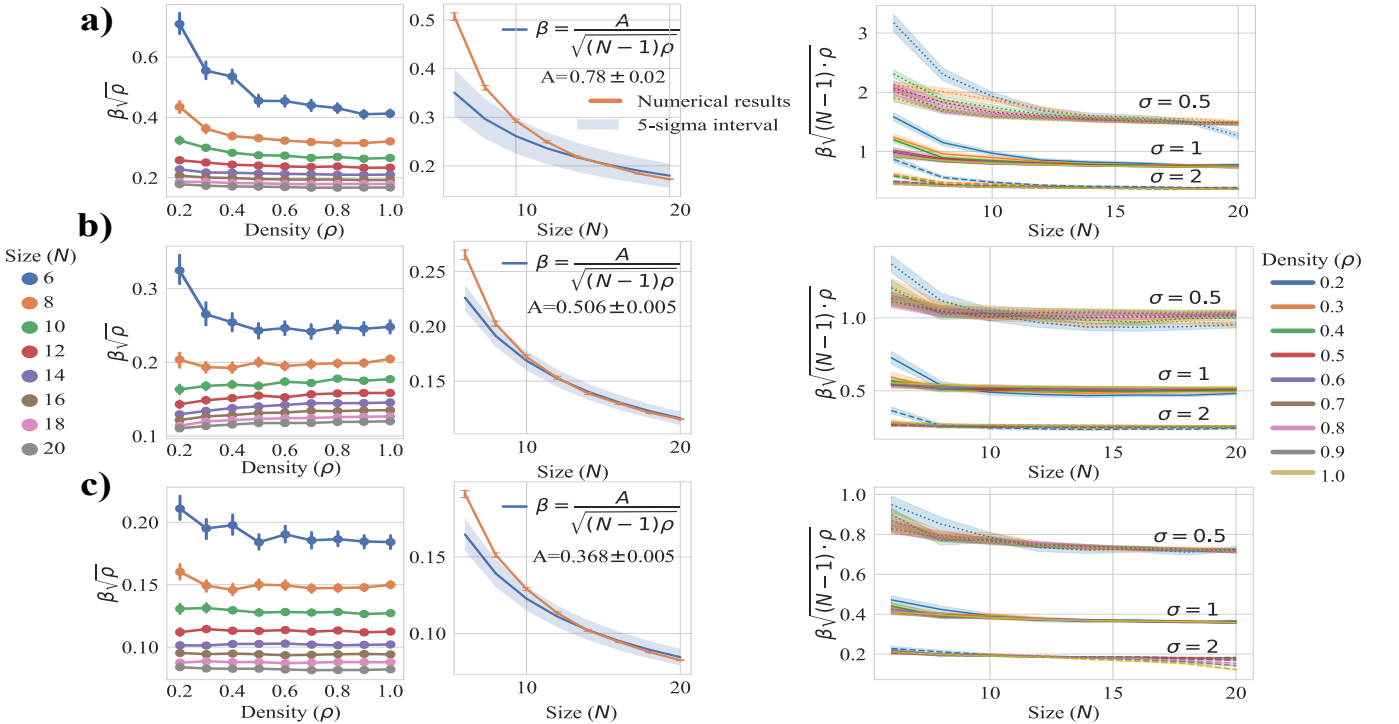


FIG. 10. Evidence that the effective temperature β after one-layer QAOA scales as $\approx \frac{\chi_\beta}{\sigma\sqrt{(N-1)\cdot\rho}} = \frac{\chi_\beta\sqrt{N}}{\sigma\sqrt{2M}}$. The results show the average of 500 instances for (a) MaxCut ($\chi_\beta = 0.78 \pm 0.02$), (b) QUBO ($\chi_\beta = 0.506 \pm 0.005$), and (c) Random Ising model ($\chi_\beta = 0.368 \pm 0.005$) problems on Gnm random graphs (Color online).

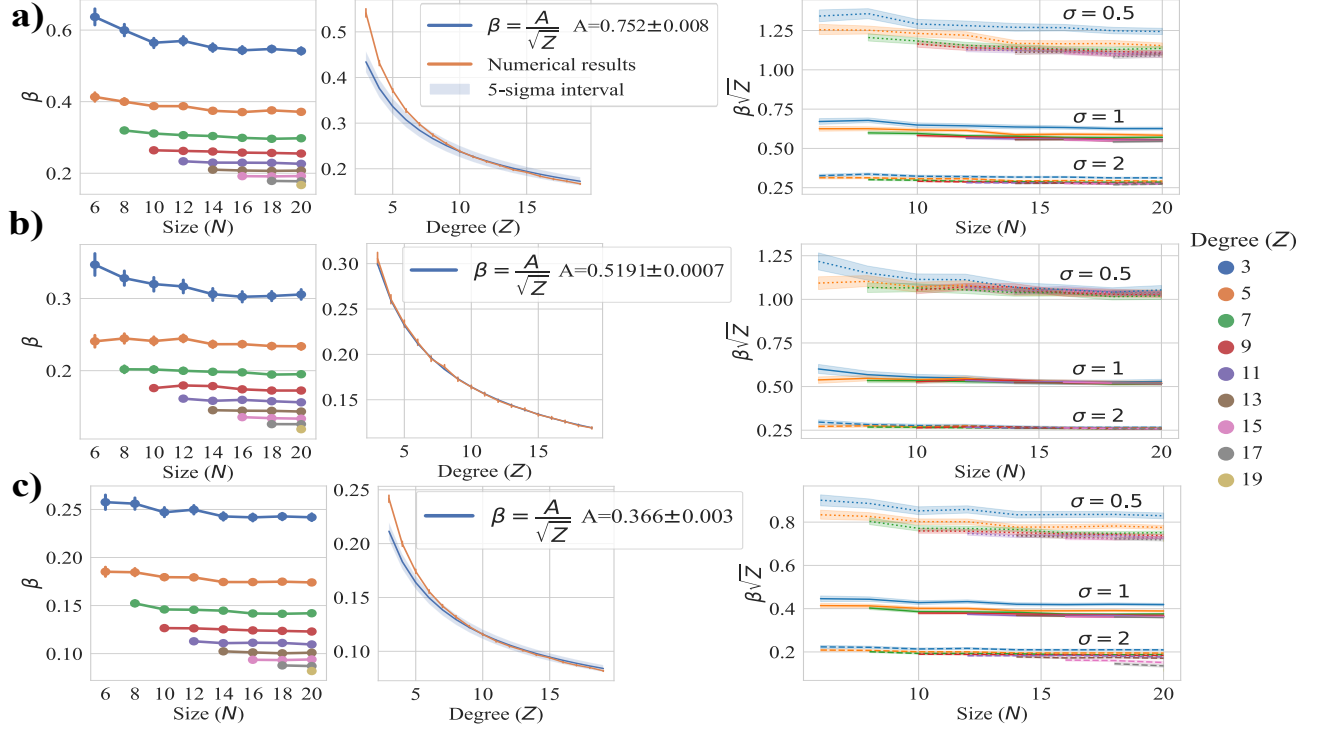


FIG. 11. Evidence that the effective temperature β after one-layer QAOA scales as $\approx \frac{\chi_\beta}{\sigma\sqrt{Z}} = \frac{\chi_\beta\sqrt{N}}{\sigma\sqrt{2M}}$. The results show the average of 500 instances for (a) MaxCut ($\chi_\beta = 0.752 \pm 0.008$), (b) QUBO ($\chi_\beta = 0.5191 \pm 0.0007$), and (c) Random Ising model ($\chi_\beta = 0.366 \pm 0.003$) problems on regular graphs (Color online).

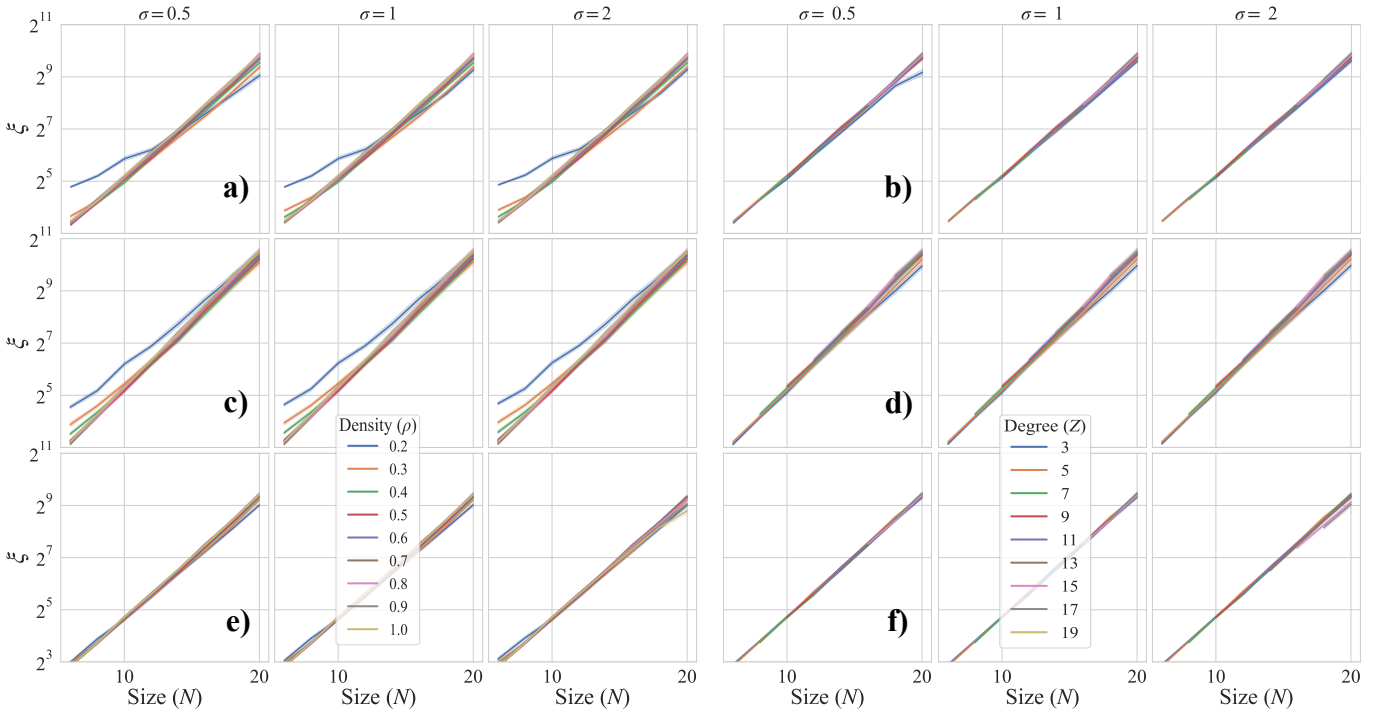


FIG. 12. Evidence that the enhancement in the ground state probability ξ of the single-layer QAOA scales as $\approx \sqrt{2^N}$. The results show the average of 500 instances and a 95% confidence interval for (a,b) MaxCut, (c,d) QUBO, and (e,f) Random Ising model problems on (a,c,e) Gnm random graphs and (b,d,f) regular graphs (Color online).